Original Research

Comparing MR Image Intensity Standardization Against Tissue Characterizability of Magnetization Transfer Ratio Imaging

Anant Madabhushi, PhD,[1] Jayaram K. Udupa, PhD,[2*] and Gul Moonis, MD[3]

Purpose: To evaluate existing methods of standardization by exploiting the well-known tissue characterizing property of magnetization transfer ratio (MTR) values obtained from MT imaging, and compare the tissue characterizability of standardized T2, proton density (PD), and T1 images against the MTR images.

Materials and Methods: Image intensity standardization is a postprocessing method that was designed to correct for acquisition-to-acquisition signal intensity variations (nonstandardness) inherent in magnetic resonance (MR) images. The main idea of this technique is to deform the volume image histogram of each study to match a standard histogram, and to utilize the resulting transformations to map the image intensities into a standard scale. The method has been shown to produce a significant gain in similarity of resulting images and to achieve numeric tissue characterization. In this work we compared PD-, T2-, and T1-weighted images before and after standardization with the corresponding MT images for 10 patient MRI studies of the brain, in terms of the normalized median values on the corresponding image histograms.

Results: No statistically significant difference was observed between the standardized PD-, T2-, and T1-weighted images and the corresponding MTR images. However, a statistically significant difference was found between the pre- and poststandardized PD-, T2-, and T1-weighted images, and between the prestandardized PD-, T2-, and T1-weighted images and the corresponding MTR images.

Conclusion: These results suggest that standardized T2, PD, and T1 images and their tissue-specific intensity signatures may be useful for characterizing disease.

Key Words: intensity standardization; standardness; MTR; image processing; tissue characterizability
J. Magn. Reson. Imaging 2006;24:667–675.

MAGNETIC RESONANCE IMAGING (MRI) is a noninvasive method for imaging the human body, and has revolutionized medical imaging. Although not commonly needed in daily clinical practice involving MR images, MR image processing, particularly segmentation and analysis (1–6), are used extensively in medical and clinical research to advance our understanding of the various diseases of the human body, as well as to diagnosis and develop strategies to treat such diseases.

A major difficulty in MR image analysis has been that intensities do not have a fixed tissue-specific numeric meaning, even within the same MRI protocol, for the same body region, or for images of the same patient obtained on the same scanner. This implies that MR images cannot be displayed at preset windows for the same protocol, body region, and application, and that window settings may have to be changed on a per-case basis. More importantly, for most postprocessing applications, such as image segmentation and quantification, this lack of a standard and quantifiable interpretation of image intensities is a major drawback that compromises the precision, accuracy, and efficiency of these applications.

A postprocessing technique to automatically adjust the contrast and brightness of MR images (i.e., windowing) for image display was presented in Ref. 7. However, although such automatic windowing may achieve display uniformity, it may not be adequate for quantitative image analysis, since the intensities still may not have tissue-specific meaning after the windowing transformation is completed. Most image analysis methods, particularly segmentation algorithms, have free parameters. Setting values for these parameters becomes very difficult without the same MRI protocol-specific intensity meaning in all images acquired as per a given protocol and for a given body region. Papers that have attempted to deal with this problem have done so from the standpoint of image segmentation and inhomogeneity correction (8,9). Guimond et al (8) described a methodology to perform three-dimensional multimodal brain image warping by using adaptive intensity correction. The core of the algorithm involves finding a transformation that maps the intensities of one image to those of another. However, this method is geared toward standardizing the intensities of only the two images that are to be registered. A previous study (9) described the use of a parametric model of the tissue

[1]Department of Biomedical Engineering, Rutgers University, New Brunswick, New Jersey, USA.
[2]Medical Image Processing Group, Department of Radiology, University of Pennsylvania, Philadelphia, Pennsylvania, USA.
[3]Division of Neuroradiology, University of Pennsylvania, Philadelphia, Pennsylvania, USA.
Contract grant sponsor: U.S. Department of Health and Human Services; Contract grant number: NS37072.
*Address reprint requests to: J.K.U., Medical Image Processing Group, Department of Radiology, University of Pennsylvania, 423 Guardian Drive, 4th Floor Blockley Hall, Philadelphia, PA 19104.
E-mail: jay@mipg.upenn.edu
Received September 21, 2004; Accepted May 4, 2006.
DOI 10.1002/jmri.20658
Published online 28 July 2006 in Wiley InterScience (www.interscience.wiley.com).

class statistics and a polynomial model of the inhomogeneity field to achieve intensity normalization and histogram adjustment. However, as was recently demonstrated (10), even the process of correcting for intensity nonuniformities that arise from field inhomogeneities can introduce its own nonstandardness in image intensities.

Some researchers have attempted to calibrate MR intensities with the help of a reference material with known MR intensity characteristics, and many such efforts were made in the early days of MRI (11,12). The main drawback of such approaches is that they cannot be used to standardize MR intensities in a post hoc setting for MR images that have already been acquired without using a standard reference material. Furthermore, in large clinical trials and routine clinical scanning of sick patients, which involve hundreds or even thousands of studies (13), any approach that does not call for the use of any reference material would be attractive. Recently, Mitchell et al (14) conducted an experiment wherein they carefully studied the effect of varying TR and TE on the resulting T2 and PD image intensity values by using reference materials of known relaxation times. In the course of that study, the authors noticed intensity nonstandardness in multiple longitudinal scans of the brain. They suggested that one could overcome this variation by carefully manually sampling regions of interest (ROIs) within the ventricular CSF region and using the mean intensity within the ROIs as a reference to linearly scale all images. Unfortunately, that study was carried out on image data from one patient, and the ROIs were specified by one operator; therefore, it is unknown how well this method will work to correct for nonstandardness (in all tissues) arising from intra-/intersubject and intra-/interscanner variations. Furthermore, as demonstrated previously (15), global linear scaling cannot correct for nonstandardness—especially when it arises from intersubject and scanner variations.

To our knowledge, the only papers that address the problem of standardization of MR intensities, based solely on the image characteristics in a post hoc manner, are Refs. 15–17. Nyul and Udupa (15) presented a method that transforms images nonlinearly so that there is a significant gain in the similarity of the resulting images. This is a two-step method wherein all images (independently of patients and the specific brand of MRI scanner used) are transformed in such a way that, for the same protocol and body region, similar intensities will yield similar tissue-specific meanings. In the first step, the parameters of the standardizing transformation are learned from a set of images. In the second step, for each MRI study, these parameters are used to map their intensity grayscale into a new grayscale. It has been shown (15–17) that standardization significantly minimizes the variation of the overall mean intensity of the MR images within the same tissue region across different studies obtained on the same or different scanners. The standardization method presented in Refs. 15 and 16 has three principal advantages over calibration methods: 1) The method does not require a reference material of known MRI property for calibration. 2) The method does not require explicit manual sampling of different tissue regions, and intensity standardization results in a usable modified image in which all tissues have standardized intensities (up to the accuracy of the method). 3) The standardization method can be applied to any MRI protocol, for any body region, and can be used to correct for intra-/interpatient, intra-/interscanner, and intra-/intersite MR image intensity variations.

Magnetization transfer (MT) imaging in MRI is based on the theory that cross-relaxation underlies the exchange of magnetization between macromolecular proton pool and freely mobile water protons (18–20). In MT imaging, two consecutive sets of images are acquired: one with off-resonance presaturation (which, for convenience, we will denote by MT1) of the relatively immobile macromolecular protons, and one without (denoted by MT2). An MT ratio (MTR) image is then computed from the MT1 and MT2 images. MTR measurements have been reproduced with less than 2% variation from site to site, and have been shown to be able to characterize tissues effectively (21,22). This provided the basic motivation for the study presented in this paper. The fundamental question we attempt to answer in this paper is the following: The tissue-specific standardness of MTR is well known and established in the literature. It has been demonstrated in the literature that, through a process of standardization, MRI protocols can be made to yield images with standard tissue-specific intensity meaning. Can we then demonstrate that standardized MRI intensities within specific tissue regions show strong correlations with MTR values within the same regions? If so, this would be another independent affirmation of the tissue-specific meaning achieved after standardization. Then, perhaps, the standardized intensities in protocols such as T2, PD, and T1 could be used as intensity signatures to distinguish between normal and diseased tissue. The standardized intensities would not provide the same physiological interpretation as the MTR, or represent the actual T1 and T2 relaxation times of tissues; however, they would have tissue-specific signatures.

MATERIALS AND METHODS

Ten multiple sclerosis (MS) patient studies, randomly selected from a large existing image database, were used in our evaluation. All MR images had been previously acquired with a 1.5-T scanner (Signa; GE Medical Systems, Milwaukee, WI, USA) with a quadrature transmitter/receiver head coil and existing protocols. The protocols consisted of axial PD- and T2-weighted imaging, and T1-weighted imaging with gadolinium enhancement (denoted from now on as T1E), and MT images. The PD-, T2-, and T1E-weighted imaging studies employed interleaved contiguous 3-mm-thick slices. The parameters for the PD and T2 protocols were as follows: TR/TE_{eff} = 2500/18 and 90 msec, echo train length = 8, number of excitations (NEX) = 1, matrix size = 256 × 256, and field of view (FOV) = 22 cm^2. For the T1E protocol TR/TE = 600/27 msec, with the other parameters as for the PD and T2 protocols. Since it takes much longer to acquire MT studies compared to the PD, T2, and T1E protocols, the corresponding MT1

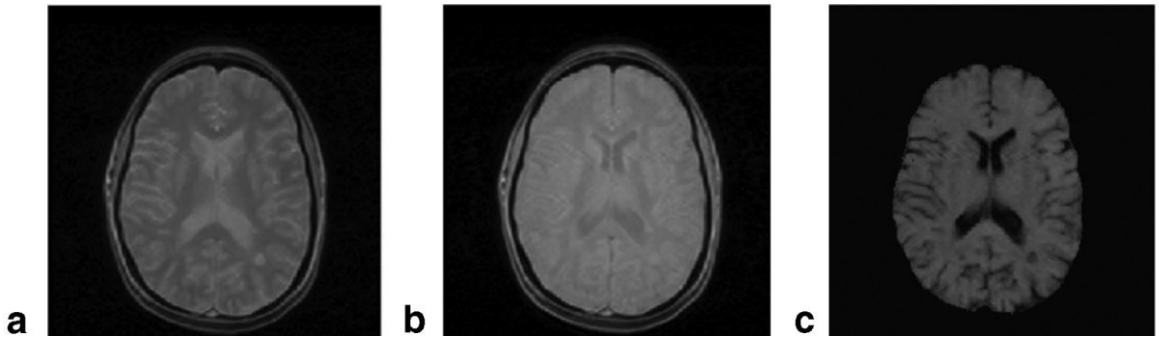

Figure 1. Corresponding slices from (**a**) C^{MT1}, (**b**) C^{MT2}, and (**c**) C^{MTR}.

and MT2 images were of lower resolution and used interleaved contiguous 5-mm-thick slices. The parameters for the MT1 and MT2 images were as follows: TR/TE = 106/5 msec, echo train length = 8, NEX = 1, matrix size = 256 × 256, and FOV = 22 cm^2. We used the 3DVIEWNIX software system (23) for image processing. All processing operations were carried out on a Pentium IV, Dell Inspiron 5100 notepad computer (2.3 GHz, 512MB RAM).

We represent a 3D volume image $\boldsymbol{C}$ (called "scene" for short) by a pair $\boldsymbol{C} = (C, f)$, where C is a finite 3D rectangular array of voxels, called the "domain of $\boldsymbol{C}$," covering a body region of the particular patient for whom scene $\boldsymbol{C}$ is acquired, and f is a function that assigns an integer intensity value $f(c)$ to each $c \in C$. Our approach consists of the following steps:

S1: Acquire a set of scenes as per the same MRI protocol π for the same body region ρ. Acquire also the corresponding MT scenes (MT1 and MT2) for the same patients for ρ.

S2: Correct for intensity nonuniformities in the MRI scenes of protocol π.

S3: Register the MRI scenes of protocol π with the MT scenes.

S4: Generate the MTR scenes from the MT scenes.

S5: Standardize the MRI scenes for each protocol π.

S6: Delineate the region corresponding to the same selected tissue t in all MRI scenes of protocol π.

S7: Compare scene intensity characteristics in tissue t, before and after standardization, for different standardization methods, with the intensity characteristics of MTR scenes in tissue t.

These steps are described in detail below.

S1: Scene Data Acquisition

We apply our method to image data obtained as per three different protocols π, namely PD, T2, T1E, and for the same body region ρ which is the brain. Thus we begin with five sets of scenes denoted by S'^{T2}, S'^{PD}, S'^{T1E}, S^{MT1}, and S^{MT2}. Each set consists of 10 scenes obtained for 10 different MS patients.

S2: Inhomogeneity Correction

We correct for background intensity inhomogeneity (arising from, among other factors, magnetic field nonuniformities) the scenes in sets S'^{T2}, S'^{PD}, S'^{T1E} to obtain new sets of scenes S^{T2}, S^{PD}, S^{T1E} by utilizing the generalized scale-based method described in Ref. 24.

S3: Registering Scenes

The scenes in S^{T2} and S^{PD} obtained for the same patient are in registration at acquisition, and so are the scenes in S^{MT1} and S^{MT2}. However, registration among other pairs of scenes (T2 and T1E, T2 and MT1, T1E and MT1) cannot be guaranteed at acquisition. Since we wish to analyze the same tissue (τ) region in all scenes, it is imperative that these pairs be registered. Because T2, PD and MT1, MT2 are registered at acquisition, only two registration operations are required (all scenes are registered with the MT scenes): T2 to MT1, and T1E to MT1. PD to MT1 registration is achieved by using the same transformation as used for T2 to MT1 registration. All registration operations utilize the mutual information method described in Ref. 25. The sets of registered and redigitized scenes corresponding to the T2, PD, and T1E scenes are denoted by S_r^{T2}, S_r^{PD}, and S_r^{T1E}, respectively.

S4: Generating the MTR Scenes

The brain is first segmented in the scenes corresponding to each patient in sets S^{MT1} and S^{MT2} by using the fuzzy connectedness method (26). This segmented brain mask is then used to compute the MTR scenes as described in Ref. 17: For each scene $\boldsymbol{C}^{MT1} = (C, f^{MT1})$ and $\boldsymbol{C}^{MT2} = (C, f^{MT2})$ in sets S^{MT1} and S^{MT2}, the MTR scene $\boldsymbol{C}^{MTR} = (C, f^{MTR})$ is computed by setting, for each voxel $c \in C$:

$$f^{MTR}(C) = \begin{cases} \dfrac{(f^{MT1}(C) - f^{MT2}(C))}{f^{MT1}(C)}, \end{cases} \quad (1)$$

Figure 1 shows the same slice from the $\boldsymbol{C}^{MT1}$, $\boldsymbol{C}^{MT2}$, and $\boldsymbol{C}^{MTR}$ scenes for one study. Note that since the background intensity inhomogeneity is generally considered to be multiplicative (27), the process of division in determining $\boldsymbol{C}^{MTR}$ from $\boldsymbol{C}^{MT1}$ and $\boldsymbol{C}^{MT2}$ eliminates its effect in the MTR scenes, and therefore no explicit correction is applied to these scenes.

S5: Standardizing the MR Image Intensity Scale

Every scene in the sets S_r^{T2}, S_r^{PD}, and S_r^{T1E} is subjected to an intensity scale standardization transformation. The

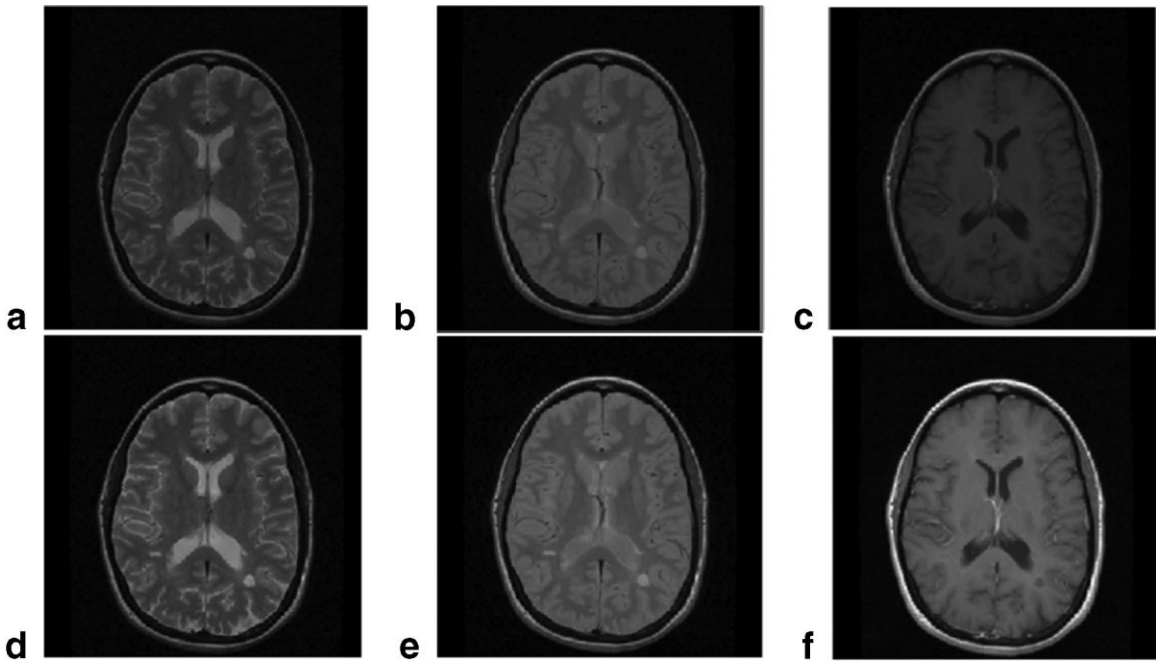

Figure 2. Matching slices from (**a**) C_r^{T2}, (**b**) C_r^{PD}, (**c**) C_r^{T1E}, (**d**) C_{rs}^{T2}, (**e**) C_{rs}^{PD}, and (**f**) C_{rs}^{T1E}.

aim of this transformation is to make the intensities of voxels containing the same tissue as similar as possible in all transformed scenes. The method is based on deforming the intensity histogram of each given scene into a standard histogram by using a nonlinear transformation, resulting in a significant gain in the similarity of the resulting images. This process is achieved in two steps: a training step that is executed only once for each given π and ρ, and a transformation step that is executed for each scene. Training and transformation are done separately for each of the three protocols in our case. In the first step, certain landmarks of a standard histogram (for each given π and ρ) are estimated from a given set of volume images. In the transformation step, the actual intensity transformation from the intensity scale of the input volume image to the standard scale is computed by mapping the landmarks to those of the standard histogram. The median intensity and other quartile locations on the histogram were used as landmarks for transforming the scene intensities. For additional details of the method, see Refs. 15 and 16. The sets of scenes corresponding to S_r^{T2}, S_r^{PD}, and S_r^{T1E} after standardization are denoted by S_{rs}^{T2}, S_{rs}^{PD}, and S_{rs}^{T1E}. Figure 2a–c show the same slice from the same patient study in S_r^{T2}, S_r^{PD},and S_r^{T1E} before standardization. The corresponding slices from sets S_{rs}^{T2}, S_{rs}^{PD}, and S_{rs}^{T1E} after standardization are shown in Fig. 2d–f. We point out here that although the order in which steps 2 and 5 is applied may seem immaterial, as demonstrated in Ref. 10, standardization should be performed only after inhomogeneity correction, since the latter step can introduce its own intensity nonstandardness.

S6: Segmenting the Same Tissue Region

To obtain the same tissue region, the scenes in set S_{rs}^{PD} were segmented for white matter (WM) by using the fuzzy connectedness method (26) and were subsequently manually corrected by an expert (neuroradiologist) when necessary. Thus, all segmentations were judged to be accurate by a trained expert. WM was utilized for quantitative evaluation, since it constitutes the largest tissue region in the brain, and the interior of this tissue region can be ascertained more reliably than other brain tissue regions, such as GM and CSF. The latter two regions have far more voxels in the tissue interface region (compared to their interior) than WM, and these are subjected to partial volume effects. The segmented tissue regions were then mapped onto the scenes in sets S_{rs}^{T2}, S_{rs}^{PD}, S_{rs}^{T1E} and S^{MTR} to obtain new sets of scenes denoted as S_{rsx}^{T2}, S_{rsx}^{PD}, S_{rsx}^{T1E} and S_x^{MTR}. The scenes in these latter sets contain intensities from the corrected, registered, and standardized scenes only within the tissue masks; elsewhere, the intensities are set to zero. In a similar manner, sets S_{rx}^{T2}, S_{rx}^{PD}, and S_{rx}^{T1E} were determined by mapping tissue masks onto the scenes in sets before standardization. Figure 3 shows the same slice from the same patient study in S_{rs}^{T2}, S_{rsWM}^{PD}, S_{rsWM}^{T1E}, and S_{WM}^{MTR}, and the WM mask (τ = WM) for this study in S_{rs}^{PD} obtained via fuzzy connectedness.

S7: Comparison With MTR

At the end of step 6 we have three groups of sets of scenes S_{rWM}^{π}, S_{rsWM}^{π}, and S_{WM}^{MTR}, where π stands for one of T2, PD, and T1E, with a total of seven sets, each containing 10 scenes. Each of these scenes constitutes a WM image of T2, PD, T1E, (before and after standardization), and MTR. Our idea is to first perform a normalization of the tissue intensities of each scene within each of the seven sets, so that they are all roughly on the same scale as the MTR. Subsequently, we compare these normalized intensity values for scenes obtained before and after intensity standardization with the normalized MTR values. We hypothesized that the normal-

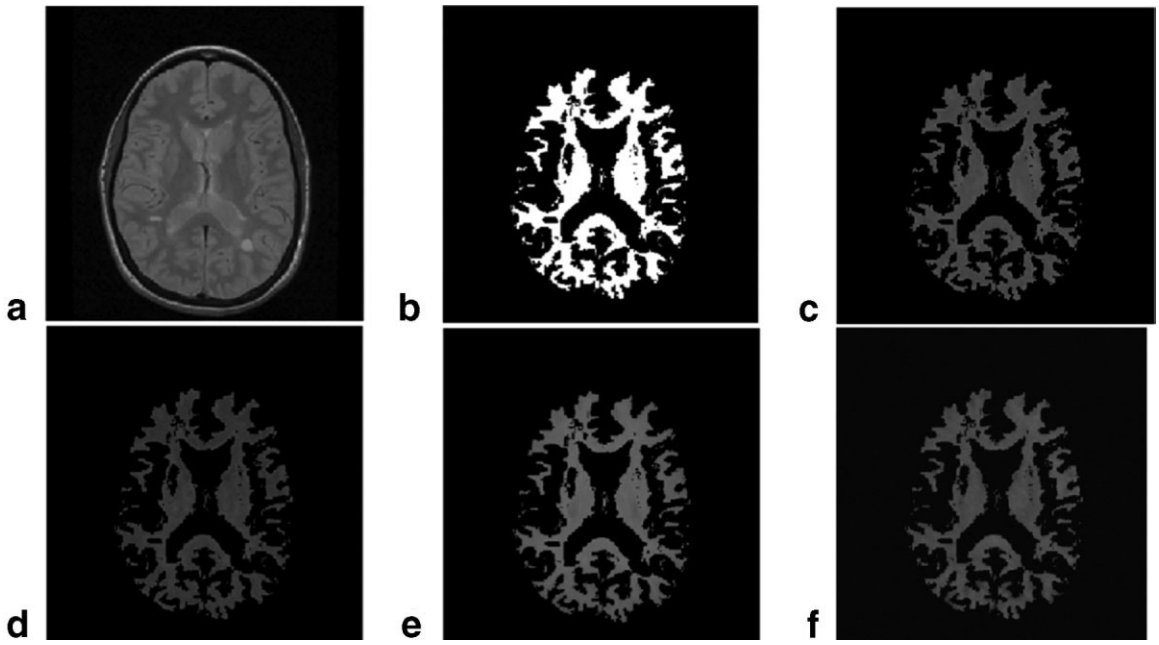

Figure 3. Matching slices from (**a**) C_{rs}^{PD}, (**b**) the WM mask obtained from C_{rs}^{PD} via fuzzy connectedness, (**c**) C_{rsWM}^{T2}, (**d**) C_{rsWM}^{PD}, (**e**) C_{rsWM}^{T1E}, and (**f**) C_{WM}^{MTR}.

ized values obtained after standardization would match the normalized MTR values significantly more closely than would values obtained before standardization. To accomplish this comparison, for each of the 70 scenes, we determine the median intensity within the WM mask, thus generating 10 median intensity values for each of the seven sets of scenes. The maximum $\mu^{\pi,\,\max}$ of the 10 median values is then determined for each of the seven sets of scenes. By using this maximum of the median values for each set, the individual median values are normalized. As an example, consider the set S_{rsWM}^{T2}. Let the maximum of the 10 median standardized T2 values in WM, obtained from this set by using the histogram-landmark-based standardization method, be $\mu_{rsWM}^{T2,\max}$. Thus each of the 10 median values μ_{rsWM}^{T2} for the set S_{rsWM}^{T2} is mapped into a new value M_{rsWM}^{T2} as follows:

$$M_{rsWM}^{T2} = \frac{\mu_{rsWM}^{T2}}{\mu_{rsWM}^{T2,\max}}. \tag{2}$$

The 10 median values in each of the seven sets S_{rWM}^{T2}, S_{rsWM}^{T2}, S_{rWM}^{PD}, S_{rsWM}^{PD}, S_{rWM}^{T1E}, S_{rsWM}^{T1E}, and S_{WM}^{MTR} are transformed in this manner. Each set of 10 normalized values in the first six sets is then compared with the set of 10 normalized median MTR values obtained from S_{WM}^{MTR} by a paired *t*-test. The set of 30 sets values coming from corresponding to sets S_{rWM}^{T2}, S_{rWM}^{PD}, S_{rWM}^{T1E} were also compared with the 10 values in S_{WM}^{MTR} by an analysis of variance (ANOVA). A similar comparison was also performed for the values in S_{rsWM}^{T2}, S_{rsWM}^{PD}, S_{rsWM}^{T1E}, and S_{WM}^{MTR}.

RESULTS

Some qualitative aspects of the results are displayed in Figs. 4–8. Figure 4a–g show the histograms of five of the 10 scenes in the sets S_{rWM}^{T2}, S_{rWM}^{PD}, S_{rWM}^{T1E}, S_{rsWM}^{T2}, S_{rsWM}^{PD}, S_{rsWM}^{T1E}, and S_{WM}^{MTR}. The low-intensity part of the histograms that corresponds to the background voxels in these scenes has been removed from the display in order to show the intensity of interest on a better scale. The histograms of the scenes before standardization are plotted in Fig. 4a–c, and the histograms of the scenes after standardization, along with the histograms of the MTR scenes, are shown in Fig. 4d–g. Figure 5a and b show the histograms of the five patient studies in Fig. 4a, but for τ = GM (sets S_{rGM}^{PD} and S_{rsGM}^{PD}). Figure 5c shows an overlay of the histograms for S_{rWM}^{PD} (Fig. 4b) and S_{rGM}^{PD} (Fig. 5a), and Fig. 5d shows the overlay of the histograms for S_{rsWM}^{PD} (Fig. 4e) and S_{rsGM}^{PD} (Fig. 5b).

Figures 6–8 show a slice from each of three PD scenes before and after standardization, and the corresponding slices from the MTR scenes for the same patient studies. Also shown in Figs. 6–8 are the slices from the corresponding binary scenes. The first binary image for the first intensity image in Figs. 6–8 was obtained by using a fixed threshold interval to segment approximately the WM region of the brain. The same threshold interval was used for the remaining two studies.

The quantitative aspects of our results are displayed in Tables 1 and 2. In Table 1 the normalized median values within WM for all 10 studies are listed for all protocols (T2, PD, and T1E) both before and after standardization. The table also shows the normalized median MTR values in WM for all studies. The *P*-values resulting from the paired *t*-test comparing the normalized median values in each of columns 1–6 with those in column 7 in Table 1 are listed in Table 2. The *P*-values resulting from the ANOVA comparing the normalized median values in each of columns 1–3 and columns 4–6 with those in column 7 in Table 1 were computed and found to be 0.019 and 0.474, respectively.

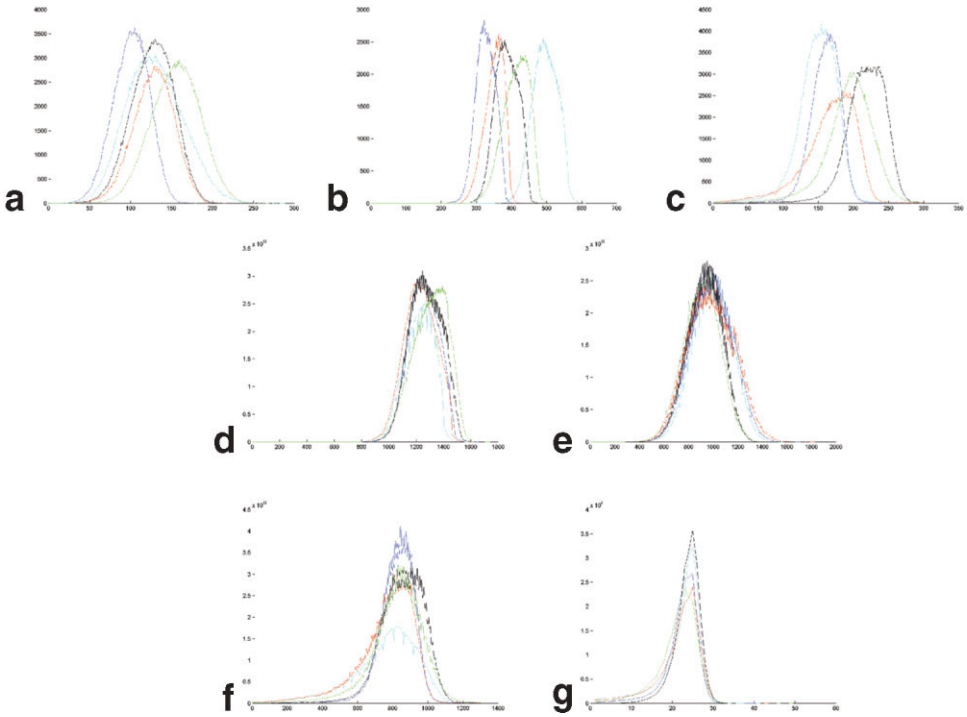

Figure 4. Histograms of scenes from the sets (**a**) S^{T2}_{rWM}, (**b**) S^{PD}_{rWM}, (**c**) S^{T1E}_{rWM}, (**d**) S^{T2}_{rsWM}, (**e**) S^{PD}_{rsWM}, (**f**) S^{T1E}_{rsWM}, and (**g**) S^{MTR}_{WM}.

DISCUSSION

Several observations can be made from the histograms in Fig. 4. Clearly, the histograms are much better aligned after standardization than before, for all three protocols (compare Fig. 4a–c with Fig. 4d–f). Further, the degree of alignment after standardization seems to be similar to the degree of alignment of MTR histograms (compare Fig. 4d–f with g). The corresponding plots for GM in Fig. 5a and b reveal that the intensity standardization method works across all tissues simultaneously. No separate tissue-specific adjustment is needed. In addition, Fig. 5c and d clearly demonstrate the numerical tissue characterizability endowed by the standardization method. The histograms for WM and GM overlap before standardization (Fig. 5c), but are clearly separated (as indicated by the dotted line) after standardization (Fig. 5d). In fact, the combined population histograms from all 10 patient studies (not shown) before standardization is quite chaotic with multiple modes, whereas standardization results in a clean unimodal histogram for each tissue region. These characteristics provide a qualitative proof of our conjecture that the intensity standardization method achieves a result similar to the inherent standard-

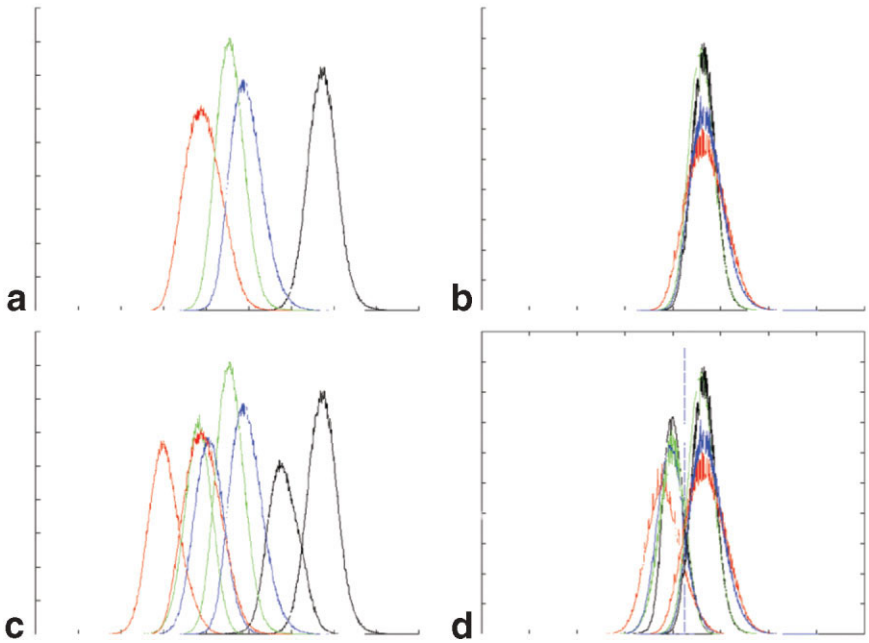

Figure 5. Histograms of scenes from the sets (**a**) S^{PD}_{rGM}, (**b**) S^{PD}_{rsWM}, (**c**) S^{PD}_{rGM} and S^{PD}_{rWM}, and (**d**) S^{PD}_{rsGM} and S^{PD}_{rsWM}. The dotted line in d shows the clear separation between the standardized histograms for GM and WM.

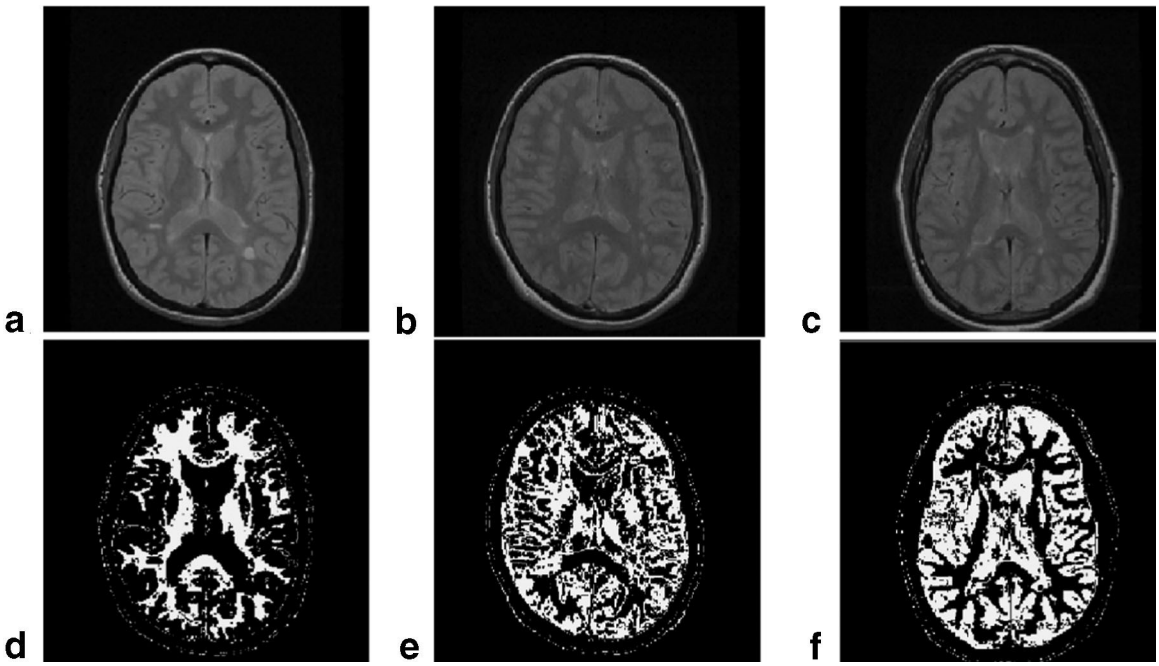

Figure 6. a–c: A slice from three different PD studies. **d–f:** Corresponding slices with the WM tissue region highlighted by using a fixed threshold interval determined for image a.

ness of MTR. Figures 6–8 provide a further qualitative proof of the numeric tissue characterizability endowed by the standardization method. In Fig. 6a (before standardization), the threshold interval chosen for this data set is appropriate to characterize numerically the WM. However, the same interval seems to characterize some WM and mostly GM in another data set displayed in Fig. 6b and e, and almost entirely the GM and some weak MS lesions in a third data set displayed in Fig. 6c and f. Upon standardization, the threshold interval derived from the first data set (Fig. 7a) excellently characterizes WM consistently in all three data sets (Fig. 7d–f). This characterizability agrees qualitatively with the manner in which MTR characterizes WM (Fig. 8d–f); however, because of poorer spatial and contrast resolu-

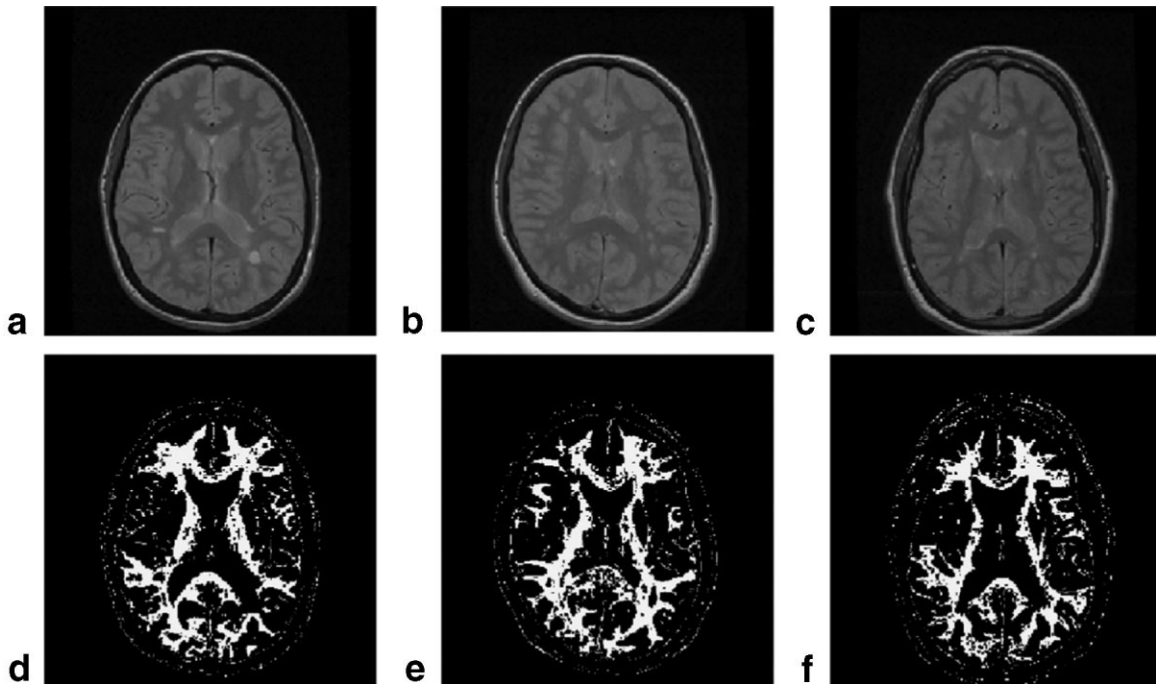

Figure 7. a–c: The same slice from the same PD studies as in Fig. 6, but after standardization. **d–f:** Corresponding slices with the WM tissue region highlighted by using a fixed threshold interval determined for image a.

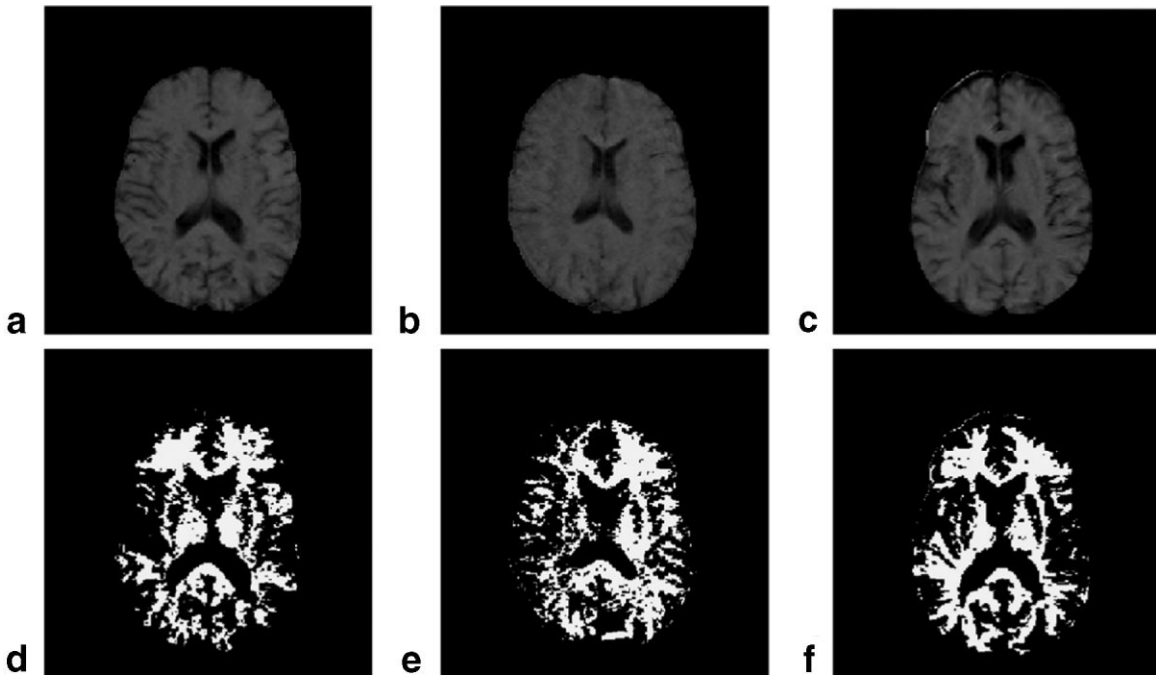

Figure 8. a–c: A slice from three different MTR studies corresponding to the patient studies in 6a–c. **d–f:** Corresponding slices with the WM tissue region highlighted by using a fixed threshold interval determined for image a.

tion in MTR, the delineation of WM by thresholding in MTR scenes is not as crisp as it is in PD scenes.

Moving now to the quantitative results displayed in Table 1, we note that the normalized median WM values seem to be more erratic and widespread (as indicated by the histograms in Fig. 4a–c) before standardization than after. This is confirmed by the *P*-values listed in the first row of Table 2. The erratic nature of the normalized median values before standardization compared to the disciplined behavior of the normalized MTR values is reflected by the *P*-values in the second row of Table 2 and the corresponding values for the ANOVA (0.019). On the other hand, the normalized median values seem to be much better disciplined after standardization than before, and seem to agree with the pattern of normalized median MTR values, as reflected by the *P*-values listed in the third row of Table 2 and the corresponding values for the ANOVA (0.474).

MR image intensity standardization methods achieve the ability of numeric tissue characterization for the commonly used MRI protocols, for different brain tissues (WM and GM) as well as for other organs (15,16). In this regard, the standardized intensities behave much like the MTR values. MTR values in the whole brain and in different tissue regions have been used in the past to characterize various neurological diseases, such as MS (18–22). Our study suggests that with standardization, commonly used anatomic MRI protocols may be utilized in a similar role. This may potentially yield information similar to that produced by MTR, but at a higher spatial and contrast resolution. Note that we are not suggesting that intensity standardized PD, T2, or T1 images would replace MT imaging, since the phenomena underlying MTR images are quite different, and MTR images have utility beyond simply possessing numerical tissue characterizability (18–20).

Table 1
Normalized Median Values in WM Before and After Standardization for the 10 Studies for T2, PD, and T1E Protocols, and the Normalized Median MTR Values for the Same Studies

Study	S_{rWM}^{T2}	S_{rWM}^{PD}	S_{rWM}^{T1E}	S_{rsWM}^{T2}	S_{rsWM}^{PD}	S_{rsWM}^{T1E}	S_{WM}^{MTR}
1	0.828	0.910	1.000	0.939	0.967	1.000	0.968
2	0.884	1.000	0.828	0.956	1.000	0.953	0.919
3	0.985	0.907	0.872	0.991	0.999	0.940	1.000
4	0.737	0.827	0.859	0.920	0.943	0.980	0.899
5	0.742	0.836	0.918	0.931	0.962	0.940	0.925
6	1.000	0.918	0.831	1.000	0.996	0.943	0.986
7	0.710	0.819	0.744	0.917	0.915	0.930	0.959
8	0.700	0.776	0.941	0.938	0.949	0.982	0.900
9	0.866	0.989	0.856	0.952	0.953	0.971	0.923
10	0.777	0.913	0.818	0.953	0.968	0.980	0.903

Table 2
P-Values of Paired *t*-Tests for Comparing the Normalized Median Signal Intensities in WM in Three Situations: Before vs. After Standardization, Before Standardization vs. MTR, and After Standardization vs. MTR.

Sets compared	π = PD	π = T2	π = T1E
$S^{\pi}_{rWM} - S^{\pi}_{rsWM}$	5.059×10^{-4}	1.725×10^{-3}	3.844×10^{-4}
$S^{\pi}_{rWM} - S^{MTR}_{rsWM}$	2.062×10^{-3}	0.040	0.010
$S^{\pi}_{rsWM} - S^{MTR}_{rsWM}$	0.389	0.141	0.125

Along similar lines, an interesting question arises as to whether the tissue characterizability of MR spectroscopy (MRS) can also be achieved via the detection of subtle differences in standardized intensities. Because anatomic MRI protocols provide higher spatial and contrast resolution, they may have higher sensitivity for tissue and disease signatures carried by segmented tissue regions than the substantially less sensitive MTR and MRS. These issues require further research. Our premise is that in many diseases, there is alteration at the microscopic level in the tissue structure. These alterations are manifested, ever so subtly, as image intensities. These signatures are lost and not detectable because of the chaotic intensity nonstandardness that is commonly present. Standardized signals may carry these subtle signatures and may help in early detection of diseases and their classification. An advantage of enhancing the sensitivity and specificity of anatomic MRI protocols is that, since they have better spatial and contrast resolution than more functional protocols, such as MTR and MRS, different tissue components can be segmented, and intensity signatures can be analyzed in tissue components. Further, one can employ computerized atlases in conjunction with MR images to analyze intensity signatures in specific functionally distinct anatomic regions.

REFERENCES

1. Bezdek JC, Hall LO, Clarke LP. Review of MR image segmentation techniques using pattern recognition. Med Phys 1993;20:1033–1048.
2. Pham DL, Xu C, Prince JL. Current methods in medical image segmentation. Ann Rev Biomed Eng 2000;2:315–338.
3. Kamber M, Shingal R, Collins DL, Francis S, Evans AC. Model-based 3-D segmentation of multiple sclerosis lesions in magnetic resonance brain images. IEEE Trans Med Imaging 1995;14:442–453.
4. Johnston B, Atkins MS, Mackiewich B, Anderson M. Segmentation of multiple sclerosis lesions in intensity corrected multi-spectral MRI. IEEE Trans Med Imaging 1996:15;154–169.
5. Zhang Y, Brady M, Smith S. Segmentation of brain MR images through a hidden Markov random field model and the expectation-maximization algorithm. IEEE Trans Med Imaging 2001:20;45–57.
6. Shen D, Herskovits EH, Davatzikos C. An adaptive-focus statistical shape model for segmentation and shape modeling of 3-D brain structures. IEEE Trans Med Imaging 2001;20:257–270.
7. Wendt RE. Automatic adjustment of contrast and brightness of magnetic resonance images. J Digital Imaging 1994;95–97.
8. Guimond A, Roche A, Ayache N, Meunier J. Three-dimensional multi-modal brain warping using the Demons algorithm and adaptive intensity corrections. IEEE Trans Med Imaging 2001;20:58–69.
9. Styner M, Brechbuhler C, Szekely G, Gerig G. Parametric estimate of intensity inhomogeneities applied to MRI. IEEE Trans Med Imaging 2000;19:153–165.
10. Madabhushi A, Udupa JK. Interplay of intensity standardization and inhomogeneity correction in MR image analysis. IEEE Trans Med Imaging 2005;24:561–576.
11. Kraft K, Fatouros P, Clarke G, Kishore P. An MRI phantom material for quantitative relaxometry. Magn Reson Med 1987;555–562.
12. Mitchell MD, Kundel HL, Axel L, Joseph P. Agarose as a tissue equivalent phantom material for NMR imaging. Magn Reson Imaging 1986;4:263–66.
13. Udupa J, Nyul LG, Ge Y, Grossman R. Multiprotocol MR image segmentation in multiple sclerosis—experience with over 1000 studies. Acad Radiol 2001;8:1116–1126.
14. Mitchell JR, Jones C, Karlik SJ, et al. MR multi-spectral analysis of multiple sclerosis lesions. J Magn Reson Imaging 1997;7:499–511.
15. Nyul LG, Udupa JK. On standardizing the MR image intensity scale. Magn Reson Med 1999;42:1072–1081.
16. Nyul LG, Udupa JK, Zhang X. New variants of a method of MRI standardization. IEEE Trans Med Imaging 2000;19:143–150.
17. Yulin G, Udupa JK, Nyul LG, Wei L, Grossman RI. Numerical tissue characterization in MS via standardization of the MR image intensity scale. J Magn Reson Imaging 2000;12:715–721.
18. Dousset V, Grossman RI, Ramer KN, et al. Experimental allergic encephalomyelitis and multiple sclerosis: lesion characterization with magnetization transfer imaging. Radiology 1992;182:483–492.
19. Grossman RI, Gomori JM, Ramer KN, et al. Magnetization transfer: theory and clinical applications in neuroradiology. Radiographics 1994;14:279–290.
20. Lexa FJ, Grossman RI, Rosenquist AC. MR of Wallerian degeneration in the feline visual system: characterization by magnetization transfer rate with histopathologic correlation. AJNR Am J Neuroradiol 1994;15:201–212.
21. van Buchem MA, Udupa JK, McGowan JC, Samarsekera S, Grossman RI. Quantification of macroscopic and microscopic cerebral disease burden in multiple sclerosis. AJNR Am J Neuroradiol 1997;18:287–1290.
22. van Buchem MA, McGowan JC, Kolson DL, Polansky M, Grossman RI. Quantitative volumetric magnetization transfer analysis in multiple sclerosis: estimation of macroscopic and microscopic disease burden. Magn Reson Med 1996;36:632–636.
23. Udupa JK, Goncalves RJ, Iyer K, et al. 3DVIEWNIX: an open, transportable, multidimensional, multi-modality, multi-parametric imaging software system. Proc SPIE 1994;2164:58–73.
24. Madabhushi A, Udupa JK, Souza A. Generalized scale: theory, algorithms, and application to inhomogeneity correction. Comput Vis Image Understand 2006;101:100–121.
25. Nyul LG, Udupa JK, Saha PK. Incorporating a measure of local scale in voxel-based 3-D image registration. IEEE Trans Med Imaging 2003;22:228–237.
26. Udupa JK, Wei L, Samarasekera S, Miki Y, van Buchem MA, Grossman RI. Multiple sclerosis lesion quantification using fuzzy-connectedness principles. IEEE Trans Med Imaging 1997;16:598–609.
27. Styner M, Brechbuhler C, Szekely G, Gerig G. Parametric estimate of intensity inhomogeneities applied to MRI. IEEE Trans Med Imaging 2000;19:153–165.